

## Synthesis, Microstructure and Electrical Properties of NiCo<sub>2</sub>O<sub>4</sub>/rGO Composites as Pseudocapacitive Electrode for Supercapacitors

Andriono Manalu<sup>1</sup>, Kerista Tarigan<sup>1\*</sup>, Syahrul Humaidi<sup>1</sup>, Masno Ginting<sup>2</sup>, Kerista Sebayang<sup>1</sup>, Martha Rianna<sup>1</sup>, Muhammadin Hamid<sup>1</sup>, Achmad Subhan<sup>2</sup>, Perdamean Sebayang<sup>2</sup>, Istas Pratomo Manalu<sup>3</sup>

<sup>1</sup> Universitas Sumatera Utara, Medan, 20155, Indonesia

<sup>2</sup> Pusat Riset Fisika, Badan Riset dan Inovasi Nasional (BRIN), Tangerang Selatan, Banten 15314, Indonesia

<sup>3</sup> Del Institute of Technology, Toba, Indonesia, 22381

\*E-mail: [kerista@usu.ac.id](mailto:kerista@usu.ac.id), [andrionomanalu@uhn.ac.id](mailto:andrionomanalu@uhn.ac.id)

Received: 2 November 2021 / Accepted: 28 December 2021 / Published: 2 February 2022

---

Pseudocapacitive type supercapacitor electrode material based on nanocomposites has been made from a mixture of NiO nanoparticles, Co<sub>3</sub>O<sub>4</sub> nanoparticles, and reduced rGO through coprecipitation and hydrothermal methods with calcination process at 900°C with variations in the composition of NiCo<sub>2</sub>O<sub>4</sub>/rGO nanocomposites at a mass ratio of nickel: cobalt: rGO, namely 2:2:2, 2:3:2, 3:2:2, 3:0:3, 0:3:3, 0:10:0 and 10:0:0. Sampling was carried out in two steps. The first step was the synthesis of NiO and Co<sub>3</sub>O<sub>4</sub> nanoparticles using NiS.5H<sub>2</sub>O and Co<sub>2</sub>SO<sub>4</sub>·7H<sub>2</sub>O precursors based on the coprecipitation method and reduced rGO derived from graphite oxide (pencil stick) using a modified hummer method. The second stage is mixing NiO, Co<sub>3</sub>O<sub>4</sub>, and rGO nanoparticles using coprecipitation and hydrothermal methods to form NiCo<sub>2</sub>O<sub>4</sub>/rGO nanocomposites which are then characterized including: physical properties with SEM, BET, and XRD, chemical properties with FTIR, thermal properties with TG/DTA, and electrical properties with CV meter. The characterization results showed that the most optimum composition was NiCo<sub>2</sub>O<sub>4</sub>/rGO nanocomposite on S2 with a mass ratio of 2:3:2 producing a hexahedron micrograph image with a spinel crystal structure with a crystalline diameter of 0.454 nm composed of the main group -OH and C=C with a wave number of 3448.51 cm<sup>-1</sup>, 1627.77 cm<sup>-1</sup>, crystallization point 468°C, mass decomposition 63.84%, specific surface area 12.75 m<sup>2</sup>/g, average pore radius 9.534 nm and pore volume 0.06404 cm<sup>3</sup>/g with its electrical performance namely electrical conductivity of 6.08 S/m and specific capacitance of 289.93 F/g which was applied as electrode candidates for pseudocapacitor type supercapacitor.

---

**Keywords:** Nanocomposite, Nickel Cobaltit (NiCo<sub>2</sub>O<sub>4</sub>), Pseudocapacitor, Reduced Graphene Oxide (rGO), Supercapacitor Electrodes

## 1. INTRODUCTION

Energy is very important in everyday life. The production and use of energy that depends on the burning of fossil fuels will greatly affect the economy and the ecology of the environment. So far, the increasing demand for environmentally friendly and high-performance renewable energy storage devices is promising. Electrochemical-based energy is one of the clean energies. The special attention that has increased in the last decade related to the world energy crisis and environmental pollution has prompted the development of electrochemical energy storage devices, such as rechargeable batteries, fuel cells and supercapacitors as energy storage systems for electric vehicles (EVs), hybrid electric vehicles (HEVs) and plug-in electric hybrid vehicles (PHEVs) [1].

Important factors for achieving high specific capacitance, energy density and power density are supercapacitor electrodes which have a large electrode surface area, high porosity, and electrical conductivity. Pseudo-capacitive materials consisting of various single metal oxides, such as  $\text{MnO}_2$ ,  $\text{NiO}$ ,  $\text{Co}_3\text{O}_4$ ,  $\text{V}_2\text{O}_5$  and  $\text{MoO}_3$  have been widely used because of the increase in specific capacitance, energy density and power density, one of which is  $\text{NiO}$ , which is very abundant in Indonesia around 8.44 million metric tons/year and includes a semiconductor material with an electrical resistivity of  $69.3 \text{ n}\Omega/\text{m}$ , an electrical conductivity of  $1.4 \times 10^7 \text{ S/m}$  and an energy gap of  $3.37 \text{ eV}$ [2]. In addition, binary or ternary transition metal oxides are very promising due to their high electrical conductivity compared to single metal oxides [3]. Binary metal oxides such as  $\text{NiCo}_2\text{O}_4$ ,  $\text{MnCo}_2\text{O}_4$ ,  $\text{CuCo}_2\text{O}_4$ , and  $\text{ZnCo}_2\text{O}_4$  are derived from cobalt oxide ( $\text{Co}_3\text{O}_4$ ) which has an electrical resistivity of  $62.4 \text{ n}\Omega/\text{m}$ , an electrical conductivity of  $1.6 \times 10^7 \text{ S/m}$  and an energy gap of  $2.8 \text{ eV} - 2.2 \text{ eV}$ [4]. The binary metal oxide material has shown excellent conductivity performance in supercapacitors. It should be noted that the electrical conductivity has the following order:  $\text{NiCo}_2\text{O}_4 > \text{Co}_3\text{O}_4 > \text{NiO}$  and many researchers have also proven that  $\text{NiCo}_2\text{O}_4$  has a much lower electrical resistance than Nickel Oxide ( $\text{NiO}$ ) and cobalt monoxide ( $\text{CoO}$ ). However, its electrochemical performance is low due to its low electrical conductivity compared to graphene oxide (rGO) materials.

The single  $\text{NiCo}_2\text{O}_4$  structure shows limited ion kinetics during redox reactions because of its low electrical conductivity or easy agglomeration on the substrate resulting in low capacitance, cycle stability and poor charge-discharge performance. Then, the bottom layer of  $\text{NiCo}_2\text{O}_4$  active material on the substrate will be difficult to react electrochemically because the diffusion of the electrolyte is inhibited at the supercapacitor electrode. Therefore, metal oxides/hydroxides, conductive polymers, metal organic frameworks (MOF) and carbon are mixed with  $\text{NiCo}_2\text{O}_4$ . Many studies have been engaged in the development of  $\text{NiCo}_2\text{O}_4/\text{rGO}$  nanocomposites as shown in Table 1.

**Table 1.** Research Development of  $\text{NiCo}_2\text{O}_4/\text{rGO}$  Nanocomposites

No	References	Topic	Findings
1	[5]	Carbon-based supercapacitors for efficient energy storage	$\text{NiWO}_4$ metal oxide deposited on $\text{NiCo}_2\text{O}_4$ can produce a specific capacitance of $1384 \text{ F g}^{-1}$ at a current density of $1 \text{ A g}^{-1}$ and cycle stability (87.6% retention over 6000 cycles).
2	[6]	Growth of $\text{NiCo}_2\text{O}_4@$ $\text{MnMoO}_4$ nanocolumn arrays	Other binary metal oxides such as $\text{MnMoO}_4$ were mixed in $\text{NiCo}_2\text{O}_4$ nanowires using the hydrothermal method, which based on

		with superior pseudocapacitor properties.	electrochemical measurements achieved a specific capacitance of 1705 F g <sup>-1</sup> and a retention of 92.6% over 5000 cycles.
3	[7]	Understanding the effect of polypyrrole and poly (3,4, ethylenedioxythiophene) on enhancing the supercapacitor performance of NiCo <sub>2</sub> O <sub>4</sub> electrodes	A conductive polymer, polypyrrole (Ppy) is an electrode material due to its good electrical conductivity (10-100 S cm <sup>-1</sup> ) and high charge density which is suitable for supercapacitor electrodes. Ppy composited with NiCo <sub>2</sub> O <sub>4</sub> has a high specific capacitance of 4.1 F cm <sup>-2</sup> at 2 mA cm <sup>-2</sup> due to the low equivalent series resistance (ESR) and the shaft and conductive properties of the Ppy material.
4	[8]	Template-engaged synthesis of uniform mesoporous hollow NiCo <sub>2</sub> O <sub>4</sub> sub-microspheres towards high-performance electrochemical capacitors.	Synthesis of NiCo <sub>2</sub> O <sub>4</sub> using chemical methods, the results obtained by electrochemical measurements reached a specific capacitance of 540 F g <sup>-1</sup> and a retention of 13% over 3500 cycles. This result has the potential as a candidate for supercapacitor electrodes.

Based on the Table 1, we found that no studies have been conducted on NiCo<sub>2</sub>O<sub>4</sub> using a mixture of citric acid through the hydrothermal synthesis method. Interestingly, the morphology, crystallinity, porosity, electrical conductivity, and electrochemical properties of NiCo<sub>2</sub>O<sub>4</sub> nanostructures will change with the addition of citric acid. Furthermore, rGO synthesized by the modified Hummer's method was mixed into a NiCo<sub>2</sub>O<sub>4</sub> solution to produce nanocomposites, where citric acid also functions as a reducing agent for rGO.

In this study, NiCo<sub>2</sub>O<sub>4</sub> will be combined with rGO to study the thermal properties, chemical properties, and electrical properties of the material so that it can be used as a candidate material for supercapacitor electrodes.

## 2. MATERIALS AND METHODS

This research uses materials consisting of Natural graphite, Nickel sulfide pentahydrate, Cobalt sulfate hydrate, Sulfide pentahydrate, Deionized water, Urea, Citric acid, Cobalt nitrate, Nickel nitrate, Hydrogen peroxide, Potassium permanganate, Hydrochloric acid, Sulfuric acid, Sodium nitrate, Zinc, and Sodium hydroxide as shown in Table 2.

**Table 2.** Research Material

No	Materials	Chemical formula	Purity	Production
1	Natural Graphite	C	99.9%	Natural
2	Nickel sulfide pentahydrate	NiS.5H <sub>2</sub> O	98%	Merck
3	Cobalt sulfate hydrate	Co <sub>2</sub> SO <sub>4</sub> .7H <sub>2</sub> O	99%	Alam
4	Sulfide pentahydrate	-	-	Merck
5	Deionized water	H <sub>2</sub> O	-	Merck
6	Urea	CH <sub>4</sub> N <sub>2</sub> O	-	Merck
7	Citric acid	C <sub>6</sub> H <sub>8</sub> O <sub>7</sub>	-	Merck
8	Cobalt nitrate	Co(NO <sub>3</sub> ) <sub>2</sub>		
9	Nickel nitrate	Ni(NO <sub>3</sub> ) <sub>2</sub>		

10	Hydrogen peroxide	H <sub>2</sub> O <sub>2</sub>	-	Merck
11	Potassium permanganate	KMnO <sub>4</sub>	-	Merck
12	Hydrochloric acid	HCl	-	Merck
13	Sulfuric acid	H <sub>2</sub> SO <sub>4</sub>	-	Merck
14	Sodium nitrate	NaNO <sub>3</sub>	-	Merck
15	Zinc	Zn	-	Merck
16	Sodium hydroxide	NaOH	-	Merck

### 2.1 Synthesis of Reduced rGO

The rGO synthesis process was carried out using a modified Hummer method. A total of 2 g of graphite powder was dissolved in 98 mL of 98% H<sub>2</sub>SO<sub>4</sub>, then 4 g of NaNO<sub>3</sub> were added during the stirring process for 1 hour. The addition of 8 g of KMnO<sub>4</sub> was carried out gradually into the mixture after stirring lasted 2 hours. For 4 hours the temperature was maintained at a temperature range of 20<sup>0</sup>C. The mixture is stirred slowly until it turns a greenish black color. The stirring process was continued for 20 hours at 35<sup>0</sup>C. After 24 hours of stirring, the mixture changed color to light brown. The mixture was washed with 200 mL of distilled water and stirred for 1 hour. After that, we remove the remaining KMnO<sub>4</sub> by added 20 mL of 30% H<sub>2</sub>O<sub>2</sub>. Furthermore, the mixture was centrifuged and continued with the washing process with 80 mL HCl and distilled water repeatedly with the aim of neutralizing the pH and reducing the remaining SO<sub>4</sub><sup>2-</sup> ions. To find out whether the SO<sub>4</sub><sup>2-</sup> ion has been used up and the pH becomes neutral, it is tested with the pp indicator. When the pH was neutral, the mixture was dried at 110<sup>0</sup>C for 12 hours to obtain graphite oxide sheets.

A total of 40 mg of graphite oxide was added to 40 ml of distilled water and stirred for 1 hour to obtain a homogeneous solution, then ultrasonication was carried out at 50/60 Hz ultrasonic waves for 90 minutes. Graphite oxide was reduced by adding 0.8 g of Zn and 10 mL of 35% HCl, then stirred for 1 hour. After 1 hour of stirring, 10 mL of 35% HCl was added to the solution and followed by a stirring process for 5-30 minutes, then washed with distilled water and 5% HCl. The washing process was carried out repeatedly using distilled water until the pH of the mixture became neutral. The precipitate from the washing process was put into a small Teflon in a stainless-steel tube and heated in a kiln at 160<sup>0</sup>C for 18 hours.

### 2.2 Synthesis of NiCo<sub>2</sub>O<sub>4</sub>

NiCo<sub>2</sub>O<sub>4</sub> nanoparticles were synthesized using the coprecipitation method by mixing the precursors NiS.5H<sub>2</sub>O and Co<sub>2</sub>SO<sub>4</sub>.7H<sub>2</sub>O as providers of Ni<sup>2+</sup> and Co<sup>2+</sup> ions with a mole fraction ratio of 1:2. The synthesis process was carried out by dissolving 1.188 grams of NiS.5H<sub>2</sub>O and 2.701 grams of Co<sub>2</sub>SO<sub>4</sub>.7H<sub>2</sub>O each into 20 mL of distilled water. The two solutions were mixed until the solution became homogeneous. Next, the solution mixture was put into 50 mL of NaOH solution (as a precipitation agent) dropwise slowly while stirring using a magnetic stirrer at 1000 rpm for 60 minutes. The solution formed is then placed on top of a permanent magnet to accelerate the deposition. The precipitate was then washed with deionized water for approximately 7 times repetitions so that the dissolved salts of other reactions

that were also dissolved in the sample were minimized to obtain a purer sample of NiCo<sub>2</sub>O<sub>4</sub> nanoparticles. After the washing process is complete, the precipitate is then dried in a furnace at a control temperature of around 90<sup>0</sup>C. This process will be successful if a brown powder is obtained.

### 2.3 NiCo<sub>2</sub>O<sub>4</sub>/rGO Nanocomposite Fabrication

In the synthesis of this nanocomposite, graphene (rG), Co(NO<sub>3</sub>)<sub>2</sub> and Ni(NO<sub>3</sub>)<sub>2</sub> were used as precursors. A total of 40 mg of rGO synthesis was added to 40 ml of distilled water and stirred for 1 hour to obtain a homogeneous solution. RGO was composited with Ni(NO<sub>3</sub>)<sub>2</sub> and Co(NO<sub>3</sub>)<sub>2</sub> with the ratio of rGO and NiCo<sub>2</sub>O<sub>4</sub> according to

Table 3, then stirred with a time variation of 2 hours at 180<sup>0</sup>C. When stirring, the solution is added with urea, citric acid and sulfide pentahydrate. The sample was then washed using deionized water until it reached a pH of 6.8-7.0. The precipitate from the washing process was put into a small Teflon in a stainless-steel tube and heated in a kiln at 160<sup>0</sup>C for 18 hours. Then the sample was calcined at 900<sup>0</sup>C for 2 hours, and the calcined powder was tested for material characterization. The number of samples of NiCo<sub>2</sub>O<sub>4</sub>/rGO nanocomposites in this study were 7 samples in which the mass composition variations used a Completely Randomized Design (CRD) with Non-Factorial and the samples were coded with a sample which is described in

Table 3.

**Table 3.** Variations in the composition of the NiCo<sub>2</sub>O<sub>4</sub>/rGO nanocomposite

Sample	Compositions
S1	NiO, Co <sub>3</sub> O <sub>4</sub> , and rGO (2 g, 2 g, 2 g)
S2	NiO, Co <sub>3</sub> O <sub>4</sub> , and rGO (2 g, 3 g, 2 g)
S3	NiO, Co <sub>3</sub> O <sub>4</sub> , and rGO (3 g, 2 g, 2 g)
S4	NiO, Co <sub>3</sub> O <sub>4</sub> , and rGO (3 g, 0 g, 3 g)
S5	NiO, Co <sub>3</sub> O <sub>4</sub> , and rGO (0 g, 3 g, 3 g)
S6	NiO, Co <sub>3</sub> O <sub>4</sub> (0 g, 10 g)
S7	NiO, Co <sub>3</sub> O <sub>4</sub> (10 g, 0 g)

The synthesized NiCo<sub>2</sub>O<sub>4</sub>/rGO nanocomposite samples were then characterized including physical properties, namely FESEM-EDS (surface morphology and elemental content), BET (specific surface area, pore volume and pore size), and XRD (crystal structure, crystal phase and crystalline diameter size).), chemical properties are FTIR (functional group), thermal properties are TG-DTA (mass decomposition and melting point), and electrical properties are CV meter (electrical conductivity and specific capacitance).

### 3. RESULTS AND DISCUSSION

#### 3.1 Characterization of Physical Properties of NiCo<sub>2</sub>O<sub>4</sub>/rGO Nanocomposites

Supercapacitor electrodes based on NiCo<sub>2</sub>O<sub>4</sub>/rGO nanocomposites have been successfully fabricated using NiS.5H<sub>2</sub>O and Co<sub>2</sub>SO<sub>4</sub>·7H<sub>2</sub>O precursors based on coprecipitation and hydrothermal methods by calcination at 900°C mixed with variations in the mass composition of NiO, Co<sub>2</sub>O<sub>4</sub> and rGO nanoparticles [9]. To prove that the NiCo<sub>2</sub>O<sub>4</sub>/rGO nanocomposite has been successfully synthesized, physical properties tests were carried out including surface morphology and elemental content with SEM-EDS, crystalline structure, and diameter with XRD and specific surface area and pore size with BET, then testing chemical properties including functional groups with FTIR, testing the thermal properties with TG/DTA and electrical properties using a CV meter [10], [11]. The formation process of NiCo<sub>2</sub>O<sub>4</sub>/rGO nanocomposite prepared using the coprecipitation method and the synthesis process of dispersed NiCo<sub>2</sub>O<sub>4</sub> nanoparticles by reduction of rGO using NiS.5H<sub>2</sub>O and Co<sub>2</sub>SO<sub>4</sub>·7H<sub>2</sub>O precursors [12], [13].

##### 3.1.1 Surface morphology analysis of NiCo<sub>2</sub>O<sub>4</sub>/rGO nanocomposites with FESEM-EDS.

Morphological image analysis of NiCo<sub>2</sub>O<sub>4</sub>/rGO nanocomposites based on compositional variations was performed using a JEOL SEM type JSM-5310 [12], [14]–[16]. Micrograph sampling by SEM was carried out by firing electrons at one point to see the surface morphology of the sample with a magnification of 20,000 times at energy of 15 kV.

Figure 1 shows the surface morphology of NiCo<sub>2</sub>O<sub>4</sub>/rGO nanocomposites synthesized by coprecipitation and hydrothermally with a calcination temperature of 900°C formed on samples S1, S2 and S3 which is seen in NiCo<sub>2</sub>O<sub>4</sub> nanoparticles has diamond-like hexahedron morphology on a thin transparent sheet (*nanosheet*) with multilayer structure and folds of the rGO layer in the form of nano flakes (*nanoflakes*) [17]. As for the elongated cylindrical-like particles that are inserted into the nanoplate in samples S1, S2 and S3, the average particle diameter is about 0.089 μm and the average particle cross-sectional area is 3.166 × 10<sup>-4</sup> μm<sup>2</sup>. Samples S4 (NiO/rGO) and S7 (NiO pure) without the addition of Co<sub>3</sub>O<sub>4</sub> compounds formed crystal structures such as nano-sized flowers (*nanoflowers*) [18]–[20] has length average of 1.022 μm, an width average of 0.785 μm and an cross-sectional area average of 0.004 μm<sup>2</sup> samples of S5 (Co<sub>3</sub>O<sub>4</sub>/rGO) and S6 on cobalt oxide (Co<sub>3</sub>O<sub>4</sub>) without the addition of nickel oxide such as small, almost spherical lumps that are uniform and aggregated with randomly distributed [21] which have length average 0.424 μm and the average width is 0.322 μm with an average surface area of 0.001 μm<sup>2</sup>.

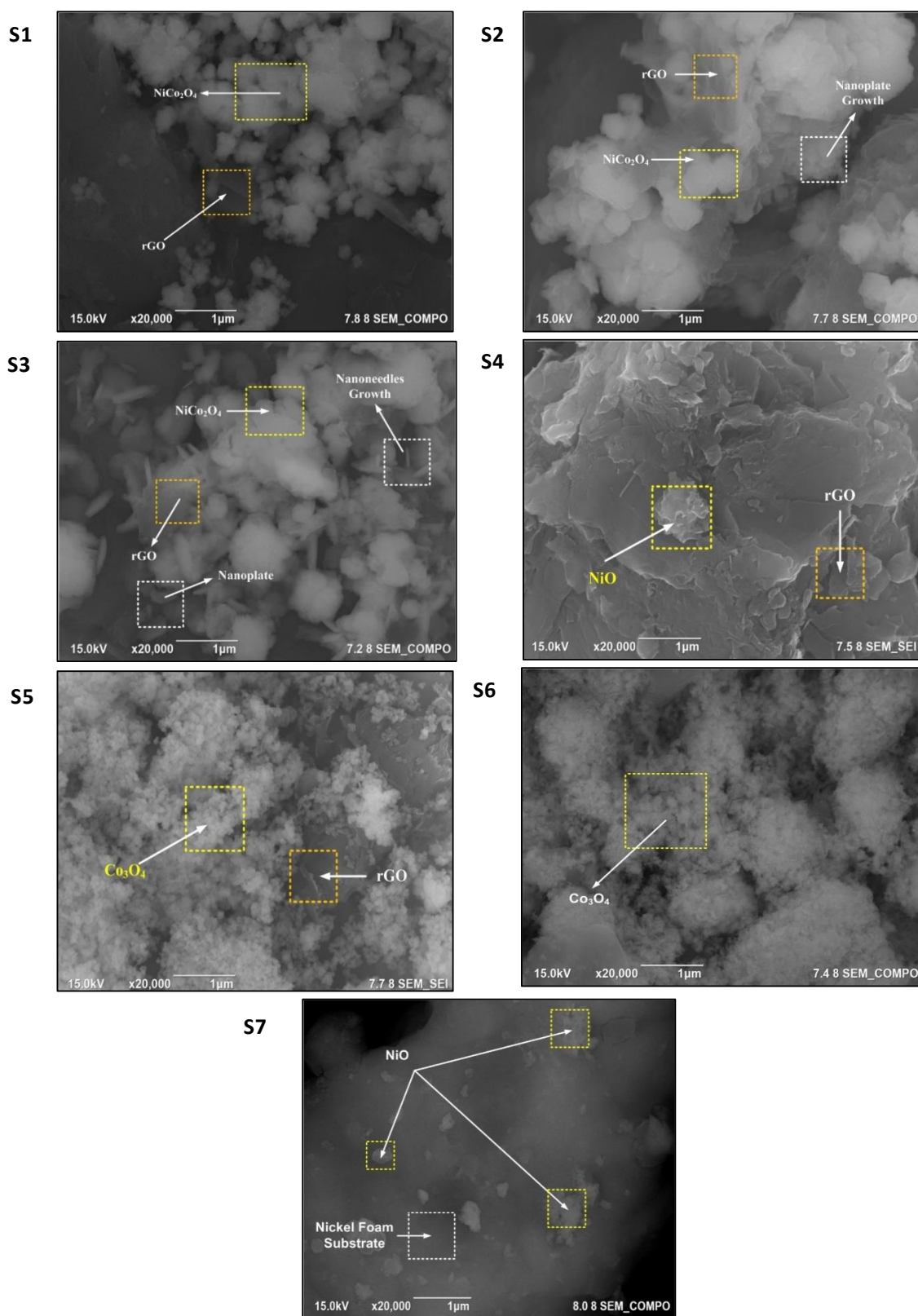


**Figure 1.** SEM Micrograph Analysis of NiCo<sub>2</sub>O<sub>4</sub>/rGO Nanocomposites at: (a) S1, (b) S2, (c) S3, (d) S4, (e) S5, (f) S6 and (g) S7 with a magnification of 20,000 times

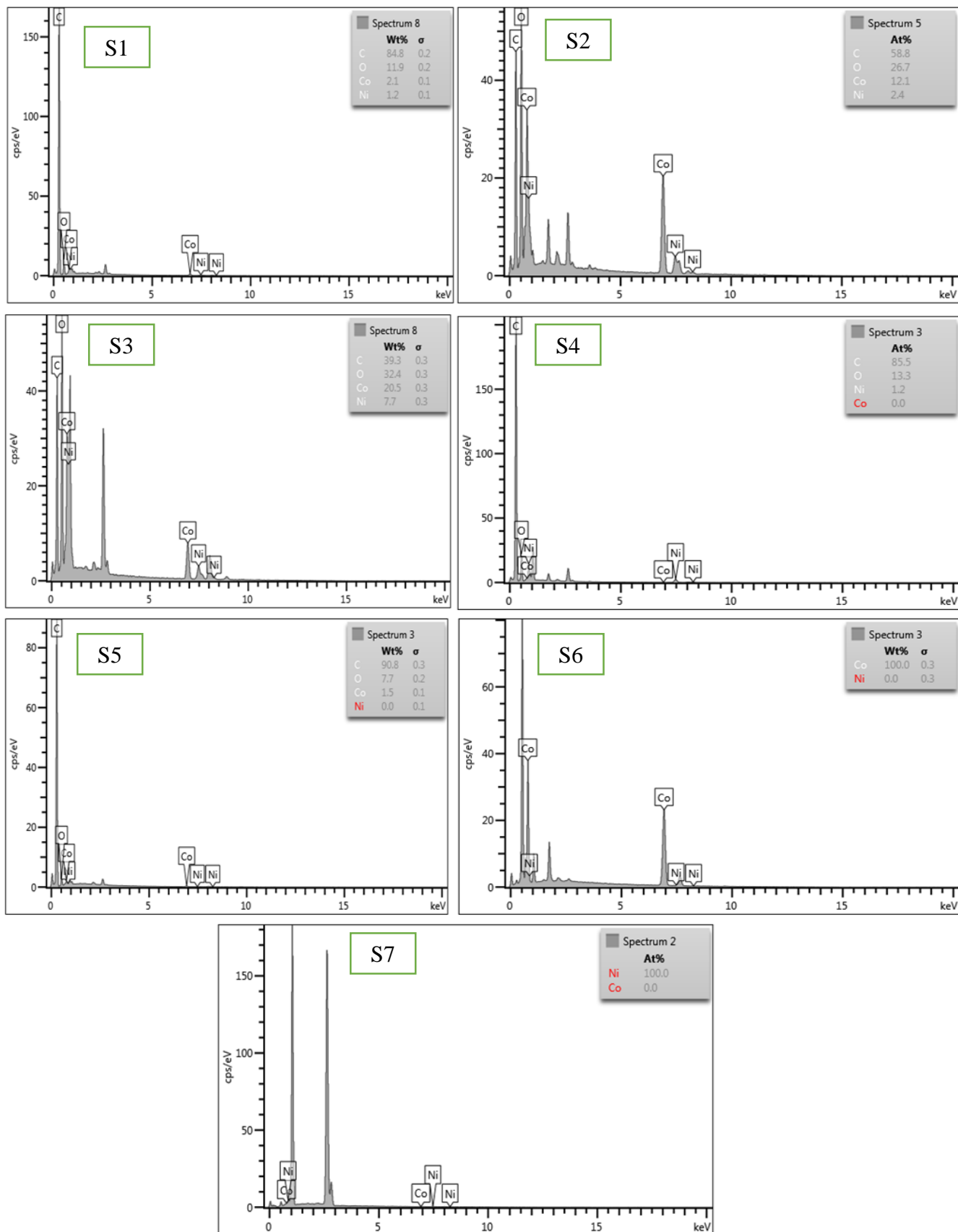


**Figure 2.** EDS test results for various compositions of NiCo<sub>2</sub>O<sub>4</sub>/rGO Nanocomposite Elements at: (a) S1, (b) S2, (c) S3, (d) S4, (e) S5, (f) S6 and (g) S7

Furthermore, EDS (Energy Dispersive Spectroscopy) test was carried out which serves to determine the levels of the dominant elements contained in samples of NiO nanoparticles,  $\text{Co}_3\text{O}_4$  nanoparticles,  $\text{Co}_3\text{O}_4/\text{rGO}$  nanocomposites, NiO/rGO and  $\text{NiCo}_2\text{O}_4/\text{rGO}$  through a graph of the relationship between elemental energy parameters (keV) on the x-axis to the intensity of counts per second (cps/counts per second) on the y-axis [18] as shown in Figure 2. Overall, the percentage of Co composition was higher than that of Ni contained in each sample S1, S2 and S3, namely 2.1% Cu, 12.1%, and 20.5%. While the element Oxygen (O) is an element forming metal oxides.

### 3.1.2 Crystal Structure Analysis with X-Ray Diffractometer

Testing the crystalline structure of  $\text{NiCo}_2\text{O}_4/\text{rGO}$  nanocomposites using a Rigaku Smartlab [22], [23] 3 kW XRD with a wavelength of Cu-K $\alpha$  radiation ( $\lambda = 1.5406 \text{ \AA}$ ) to observe the sample from a diffraction angle ( $2\theta$ ) =  $5^\circ - 90^\circ$  at a scan speed of  $2^\circ \text{ min}^{-1}$ , voltage 44 kV, and current 40 mA. Figure 3 shows that the result of the analysis of the crystalline structure for the  $\text{NiCo}_2\text{O}_4/\text{rGO}$  nanocomposite which is shown by the diffraction pattern.

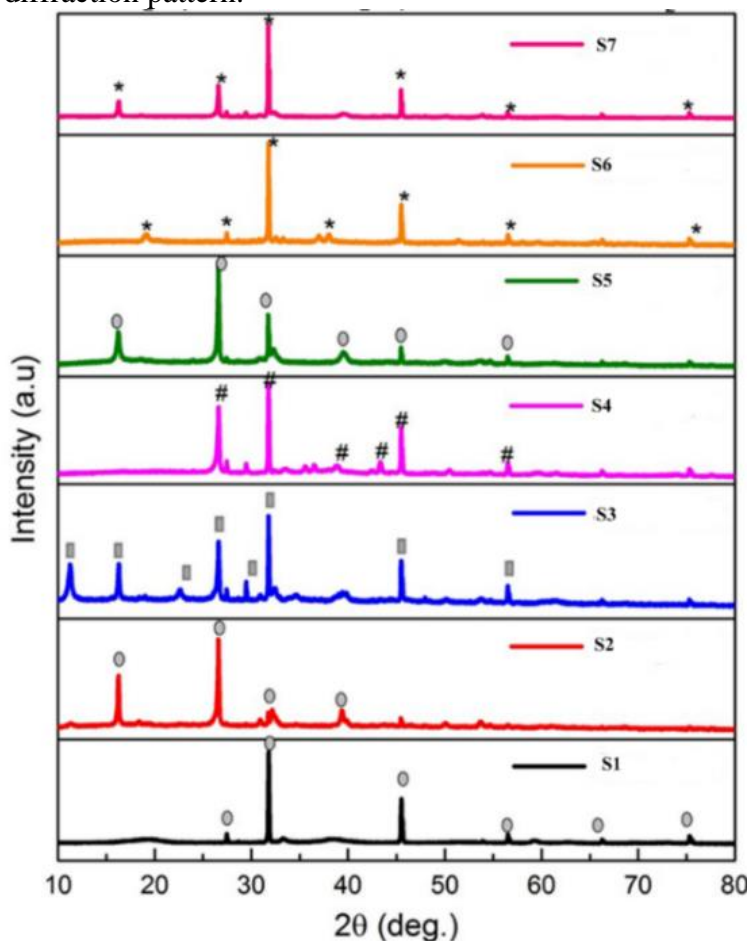


**Figure 3.** Diffraction Pattern (XRD) on  $\text{NiCo}_2\text{O}_4/\text{rGO}$  Nanocomposite

Comparison of the diffraction pattern of 100%  $\text{Co}_3\text{O}_4$  (S6) nanoparticles before being mixed with rGO and nickel oxide, and 100% NiO (S7) before being mixed with rGO and cobalt oxide with the diffraction pattern of the combined results of NiO,  $\text{Co}_3\text{O}_4$  with rGO in the manufacture of  $\text{Co}_3\text{O}_4/\text{rGO}$

nanocomposites (S5), NiO/rGO (S4) and NiCo<sub>2</sub>O<sub>4</sub>/rGO (S1, S2 and S3) with compositions using coprecipitation and hydrothermal methods for a calcination temperature of 900°C. In samples S4 and S7, NiO dominates in the nanocomposite because NiO is present at the highest peak of the XRD diffraction pattern.

**Table 4.** Analysis of the Highest Peak Result of the Diffraction Pattern of NiCo<sub>2</sub>O<sub>4</sub>/rGO Nanocomposites

Sample	Peak of-	2θ (deg)	d (Å)	hkl
NiCo <sub>2</sub> O <sub>4</sub> /rGO (S1)	1	31.69	2.8212	[2 0 0]
	2	45.42	1.9952	[1 1 1]
	3	45.54	1.9903	[2 2 0]
NiCo <sub>2</sub> O <sub>4</sub> /rGO (S2)	1	16.24	5.4535	[1 0 1]
	2	26.59	3.3496	[2 2 0]
	3	32.15	2.7819	[2 0 4]
NiCo <sub>2</sub> O <sub>4</sub> /rGO (S3)	1	26.53	3.3571	[2 0 0]
	2	31.70	2.8204	[2 2 0]
	3	45.43	1.9948	[2 2 0]
NiO/rGO (S4)	1	31.77	2.8143	[1 0 1]
	2	45.50	1.9919	[1 3 0]
	3	56.51	1.6272	[2 0 0]
Co <sub>3</sub> O <sub>4</sub> /rGO (S5)	1	16.17	5.4770	[1 0 0]
	2	26.53	3.3571	[2 2 0]
	3	32.19	2.7785	[1 2 0]
Co <sub>3</sub> O <sub>4</sub> (S6)	1	31.81	2.8109	[1 0 1]
	2	45.66	1.9853	[2 0 0]
	3	56.72	1.6216	[2 0 2]
NiO (S7)	1	31.81	2.8109	[2 0 0]
	2	45.66	1.9853	[2 2 0]
	3	59.24	1.5585	[2 1 1]

Table 4 can be analyzed that there is a change in the value of the diffraction angle of 2θ and the distance between planes (d) of NiO, Co<sub>3</sub>O<sub>4</sub>, and rGO which have been modified into NiCo<sub>2</sub>O<sub>4</sub>/rGO composites. Changes in the value of the diffraction angle of 2θ indicate an interaction between Ni<sup>2+</sup> cations from NiO and Co<sup>2+</sup> from Co<sub>3</sub>O<sub>4</sub> with GO<sup>-</sup> anions from rGO, resulting in the attraction of Co<sub>2</sub>O<sub>4</sub> and rGO by the NiO matrix. It is verified that there is Co<sub>3</sub>O<sub>4</sub> and rGO in the NiCo<sub>2</sub>O<sub>4</sub>/rGO nanocomposite. In addition, it can be seen that NiCo<sub>2</sub>O<sub>4</sub> is located in almost all the peaks of the nanocomposite diffraction pattern at S1, S2, and S3 very dominating and there is agreement with the standard data from JCPDS No. 20-0781 which indicates that the crystal structure for NiCo<sub>2</sub>O<sub>4</sub> is spinel and has a *cubic* phase where the orientation of the crystal planes are [2 2 0] and [1 1 1].

However, the peak of the diffraction pattern for rGO is not clearly visible due to a change in the structure to amorphous due to hydrothermal treatment with 900°C calcination which causes a decreased crystallinity level, resulting in the appearance of graphite oxide peaks during the reduction process so

that it becomes an impurity in the rGO material. Meanwhile, S4, S5, S6 and S7 produce diffraction peaks indicating NiO and Co<sub>3</sub>O<sub>4</sub> compounds for NiO according to JCPDS 47-1049 having a monoclinic crystal structure with a cubic phase having a crystal plane orientation [2 0 0] while Co<sub>3</sub>O<sub>4</sub> according to JCPDS 42-1467 has a cubic spinel crystal structure with a crystal plane orientation [2 2 0].

Through the XRD diffraction pattern, the size of the crystalline diameter (D) is obtained by calculating the FWHM. FWHM is converted to radians by multiplying /180 by ( $\pi = 3.14$ ). Determination of the Bragg angle ( $\theta$ ) is obtained from the FWHM value from the results of the Match analysis as follows:

$$D = \frac{k\lambda}{B_0 \cos \theta} \quad (3.1)$$

With  $k$  = shape factor constant value or Scherrer determination ( $k = 0.9$ ),  $B_0$  = FWHM value,  $\lambda$  = X-ray wavelength used, namely cathode  $\lambda$  CuK $\alpha$  = 1.541874Å and  $\theta$  = X-ray diffraction angle fired at the maximum peak ( $^\circ$ ). The result can be shown as follows:

**Table 5.** Diameter Size of NiCo<sub>2</sub>O<sub>4</sub>, NiO, and Co<sub>3</sub>O<sub>4</sub> Crystalline Crystals Distributed in NiCo<sub>2</sub>O<sub>4</sub>/rGO Nanocomposite Samples

Sample	2 $\theta$ (deg)	FWHM (rad)	D (nm)
S1	45.42	0.08	0.0178
S2	26.59	0.18	0.454
S3	31.7	0.1	0.826
S4	56.51	0.14	0.644
S5	26.53	0.16	0.511
S6	45.66	0.08	0.0108
S7	45.66	0.1	0.862

Table 5 can be concluded for NiCo<sub>2</sub>O<sub>4</sub> nanoparticles, the average crystalline diameter is 0.4326 nm, for NiO nanoparticles synthesized by coprecipitation using NiS.5H<sub>2</sub>O precursors, the average crystalline diameter of 0.753 nm and for Co<sub>3</sub>O<sub>4</sub> nanoparticles synthesized from Co<sub>2</sub>SO<sub>2</sub>·7H<sub>2</sub>O precursors has an average crystalline diameter of 0.2609 nm.

### 3.1.3 Surface Area Analysis of NiCo<sub>2</sub>O<sub>4</sub>/rGO nanocomposites using BET and pore size distribution using BJH

BET test analysis was carried out to determine the specific surface area and pore size distribution of BJH (*Barrett–Joyner–Halenda*) NiCo<sub>2</sub>O<sub>4</sub>/rGO nanocomposites including the average atomic radius and hole volume using the Sorption machine [24].

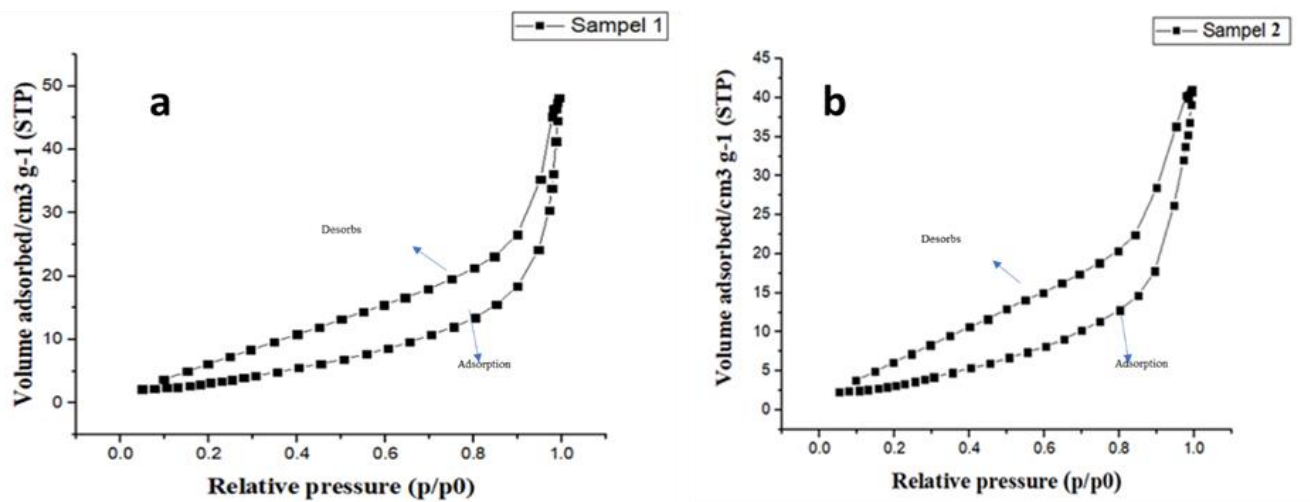


**Figure 4.** BET Analysis on the Adsorption-Desorption Isotherm Reaction of N<sub>2</sub> Nanocomposite NiCo<sub>2</sub>O<sub>4</sub>/rGO at: (a) S1 and (b) S2

Based on Figure 4, the results of the BET test can be analyzed that the isotherm reaction process shows the characteristic behavior of the pores of the NiCo<sub>2</sub>O<sub>4</sub>/rGO nanocomposite sample in absorbing and releasing (adsorption-desorption) dinitrogen gas molecules (N<sub>2</sub>) resulting in a hysteresis loop with a larger relative pressure range (P/P<sub>0</sub>) for samples S1 and S2, respectively, 0.1–0.95 P/P<sub>0</sub> and 0.12–0.99 P/P<sub>0</sub>. This indicates the presence of mesopores that may be formed from sheets of the NiCo<sub>2</sub>O<sub>4</sub>/rGO nanocomposite structure that are loose or peeling from the layer on the stack of nanoparticles [25].

**Table 6.** Characterization Results of Specific Surface Area, Average Pore Radius and Total Volume of NiCo<sub>2</sub>O<sub>4</sub>/rGO Nanocomposite Material

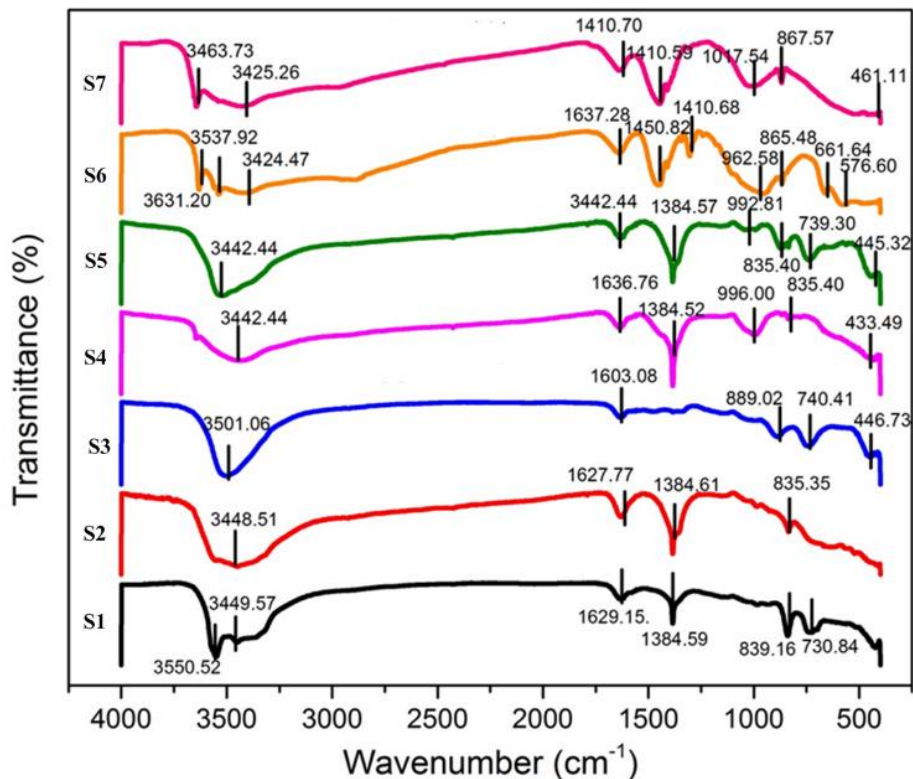
Sample	Average Specific Surface Area (m <sup>2</sup> /g)	Average Pore Radius (Å)	Pore Volume (cm <sup>3</sup> /g)
S1	12.90	109.77	0.07455
S2	12.75	95.34	0,06304

Table 6 shows that the pore size is uniformly distributed on the surface of the nanocomposite, namely the mesoporous size range between 2 nm – 50 nm which at S1 and S2 respectively produces an average pore radius of 109.77 and 95.34 or equivalent to 10.977 nm and 9.534 nm. While the specific surface area of BET at S1 and S2 are 12.90 m<sup>2</sup>/g and 12.75 m<sup>2</sup>/g. And the pore volumes of BJH desorption at S1 and S2 were 0.00745 cm<sup>3</sup>/g and 0.6304 cm<sup>3</sup>/g.

*3.1.4 Characterization of the chemical properties of NiCo<sub>2</sub>O<sub>4</sub>/rGO nanocomposites using FTIR functional group analysis*

From the results of the FTIR spectrum analysis of NiCo<sub>2</sub>O<sub>4</sub>/rGO nanocomposites as shown in Figure 5, it can be concluded that for S1, S2 and S3 there are strong and wide absorption bands at wave

numbers 3550.52 cm<sup>-1</sup>, 3448.51 cm<sup>-1</sup> and 3501.44 cm<sup>-1</sup> which indicate overlapping of the vibrational range of the –OH group. In the IR spectra of the prepared nanocomposite as shown in on the Table 7, C-H vibrations from alkanes also appeared at wave numbers 1384.59 cm<sup>-1</sup>, and 1384.61 cm<sup>-1</sup>. While the absorption band at wave numbers 839.16 cm<sup>-1</sup>, 835.35 cm<sup>-1</sup> and 889.02 cm<sup>-1</sup> shows the bending of the Co-OH group. As well as the formation of NiCo<sub>2</sub>O<sub>4</sub> nanocomposites indicated by absorption bands at waves around 730.84 cm<sup>-1</sup>, 740.41 cm<sup>-1</sup> and 446.73 cm<sup>-1</sup> which indicate the occurrence of stretching vibrations in the Ni-O and Co-O bonds.



**Figure 5.** Analysis of FTIR Spectra on NiCo<sub>2</sub>O<sub>4</sub>/rGO Nanocomposites against S1 to S7

**Table 7.** Differences in IR Absorption of NiCo<sub>2</sub>O<sub>4</sub>/rGO Nanocomposites against S1 to S7

Nanocomposite Sample Wave Number NiCo <sub>2</sub> O <sub>4</sub> /rGO (cm <sup>-1</sup> )							Reference Wave Number (cm <sup>-1</sup> )	Reference Vibration
S1	S2	S3	S4	S5	S6	S7		
3550	3448	3501	3442	3442	3424	3425	3200 – 3600	-OH intermolecular of primary alcohol
1629	1627	1603	1636	1642	1637	-	1610-1680	Vibration C=C from Alkene
1384	1384	-	1384	1384	1450	1410.7	1340-1470	CH Range of Alkanes
-	-	-	996	992	962	-	900 – 1050	-CH range of alkene vibrations (CH <sub>3</sub> )
839	835	889	835	-	865	867	800 – 950	Range Co-O
730	-	740	-	739	-	-	665 – 795	Range Ni-O
-	-	-	-	-	576	-	480 – 650	Vibration bending Co-OH
-	-	446	433	445	-	461.11	<500	Vibration Stretch Ni-O

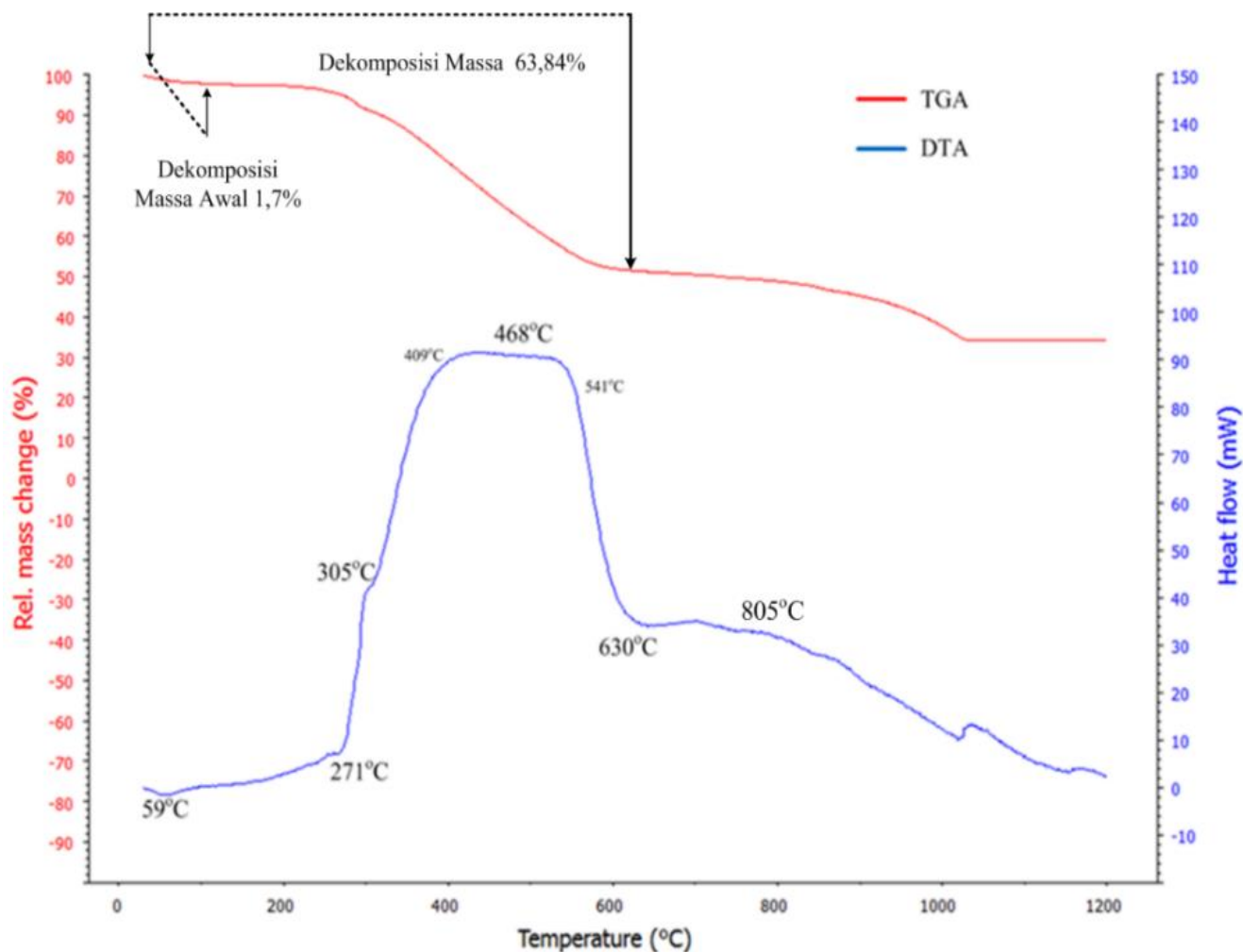


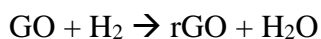
**Figure 6.** Analysis of TG/DTA curves on NiCo<sub>2</sub>O<sub>4</sub>/rGO Nanocomposites against S1

These results when compared with S4, S5, S6 and S7 nanocomposites basically show similarities in their functional groups due to the addition of rGO in this case as a substance that stabilizes the formation of NiCo<sub>2</sub>O<sub>4</sub>/rGO nanocomposites and functions as a dopant[26]. In addition, the presence of rGO does not necessarily change the chemical structure of the NiCo<sub>2</sub>O<sub>4</sub>/rGO nanocomposite. This is consistent with the results of the FTIR characterization that there is no change or shift in the wave number in the IR spectra.

### 3.1.5 Thermal Properties Characteristics of NiCo<sub>2</sub>O<sub>4</sub>/rGO Nanocomposites using TG/DTA analysis

The thermal properties of the NiCo<sub>2</sub>O<sub>4</sub>/rGO nanocomposite were determined by the TG/DTA method [24] using a Linseis type TA PT 1600 device where the test sample was heated from 0°C to 1200°C with a heating speed of 10°C/min. As shown in the *Figure 6* The TG-DTA curve of sample S1 shows that on the DTA curve there is an endothermic peak at a temperature of about 59°C where the composition of the absorber material begins to absorb heat with a large amount of heat energy absorbed, which is 1.109 Joules, which is this phenomenon followed by a weight loss of about 1.7% shown by the

TGA. We found that one of the reactions is the decomposition of Ni(OH)<sub>2</sub> and Co(OH)<sub>2</sub> into NiO, CoO and H<sub>2</sub>O:



This phenomenon no significant gradual weight loss was observed on the TGA curve and indicated late phase formation in both compounds. Then the endothermic process occurs again at a temperature of around 305°C with absorbed heat energy of 148.25 J which results in dehydration and elimination of volatile components so that Ni<sub>2</sub>O<sub>3</sub> and Co<sub>2</sub>O<sub>4</sub> compounds begin to release oxygen functional groups (O<sub>2</sub>) and a reduction reaction occurs as follows:



The strong peak is due to the decomposition of the NiCo<sub>2</sub>O<sub>4</sub> precursor and indicates a solid reaction between NiO and Co<sub>3</sub>O<sub>4</sub> or the formation of NiCo<sub>2</sub>O<sub>4</sub>, as shown by the equation:



In the exothermic reaction, the decomposition of the weight change is shown on the TGA curve, which is 63.84%. While at a temperature of 630°C the rGO carbon skeleton burns which are the point of phase transformation. While the temperature of 783°C of the nanocomposite material began to damage the spinel structure of NiCo<sub>2</sub>O<sub>4</sub> which is the melting point of the precursor compounds NiS.5H<sub>2</sub>O and Co<sub>2</sub>SO<sub>4</sub>.7H<sub>2</sub>O. The results of the literature from Pub.Chem that the melting point value for NiS compounds are 797°C while for Co<sub>2</sub>SO<sub>4</sub> compounds are 735°C.

### 3.2 Characterization of Electrical Properties of NiCo<sub>2</sub>O<sub>4</sub>/rGO Nanocomposites CV Meter Analysis.

#### 3.2.1 Electrical Conductivity Properties Analysis

The results of testing the electrical conductivity properties using the CV meter method with the GW-Instek 816 series engine based on RC circuits in the frequency range of 1 kHz - 300 kHz. The electrical conductivity curve of the NiCo<sub>2</sub>O<sub>4</sub>/rGO nanocomposite against samples S1 to S7 as shown on the

Table 8, each of which has an average electrical conductivity for pure NiO nanoparticles (S7) 1,36 x 10<sup>-3</sup> S/m, pure Co<sub>3</sub>O<sub>4</sub> nanoparticles (S6) 2,8 x 10<sup>-3</sup> S/m, then for the Co<sub>3</sub>O<sub>4</sub>/rGO (S5) nanocomposite it was 1.23 S/m and the NiO/rGO (S4) nanocomposite was 5,871 S/m. While the results of combining NiO nanoparticles, Co<sub>3</sub>O<sub>4</sub> nanoparticles and rGO into NiCo<sub>2</sub>O<sub>4</sub>/rGO nanocomposites resulted in an average electrical conductivity for samples S1 which was 2.19 S/m, S2 was 6.08 S/m and S3 was 3.64 S/m. So, it can be concluded that the best conditions are in the NiCo<sub>2</sub>O<sub>4</sub>/rGO nanocomposite code sample S2 while the unfavorable conditions are in the sample code S1.

**Table 8.** Characterization Results of the Electrical Conductivity Values of NiCo<sub>2</sub>O<sub>4</sub>/rGO Nanocomposites against S1

Sample Code	Electrical Conductivity (S/m)
S1	2.19
S2	6.08
S3	3.64
S4	5.871
S5	1.23
S6	2.8 x 10 <sup>-3</sup>
S7	1.36 x 10 <sup>-3</sup>

Based on

Table 8, it can be concluded that NiCo<sub>2</sub>O<sub>4</sub>/rGO nanocomposites can be used as electrode materials for pseudocapacitive supercapacitors because the electrical conductivity standard for electrochemical supercapacitors (pseudocapacitors) has a range of = (0.1 – 1) S/m[27]. It had fewer holes that could accelerate free electrons to move. This has been proven from the results of XRD and BET tests which show that sample S2 has a crystalline diameter of 0.454 nm, an average pore radius of 95.34 Å or equivalent to 9.534 nm, a specific surface of BET 12.75 m<sup>2</sup>/g, and BJH desorption pore volume was 0.6304 cm<sup>3</sup>/g.

### 3.2.2 Capacitance Properties Analysis

Capacitance testing is carried out using a 3-electrode setup on CV in an RC circuit. Where the capacitance value can be obtained from the impedance equation which is formulated as follows: [28]

$$Z = \frac{R}{1 + (R^2 \omega^2 C_{RLC}^2)}$$

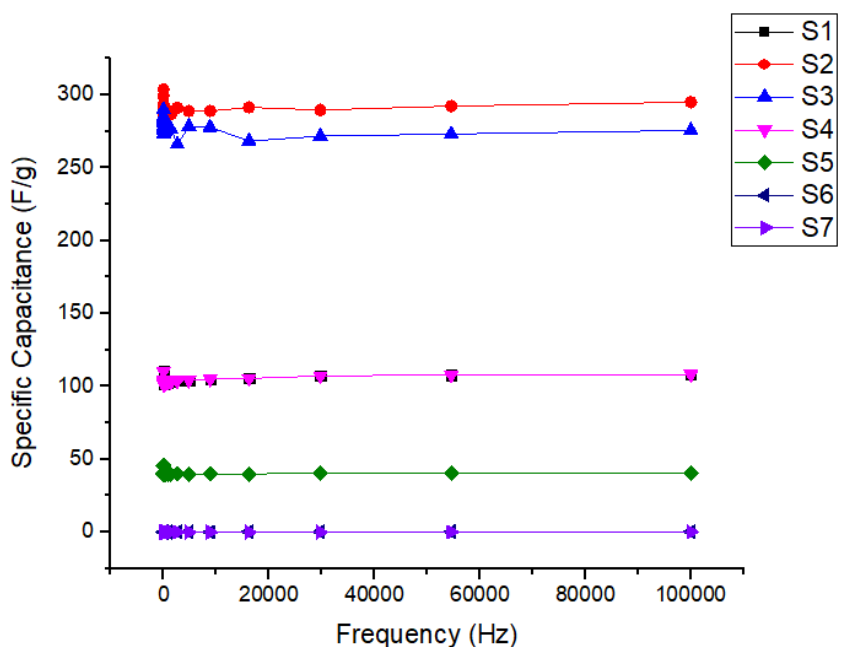
$$C = \frac{I \cdot t}{\Delta V}$$

$$C_{Total \text{ Pseudocapacitor}} = C + C_{RLC} \quad (3.2)$$

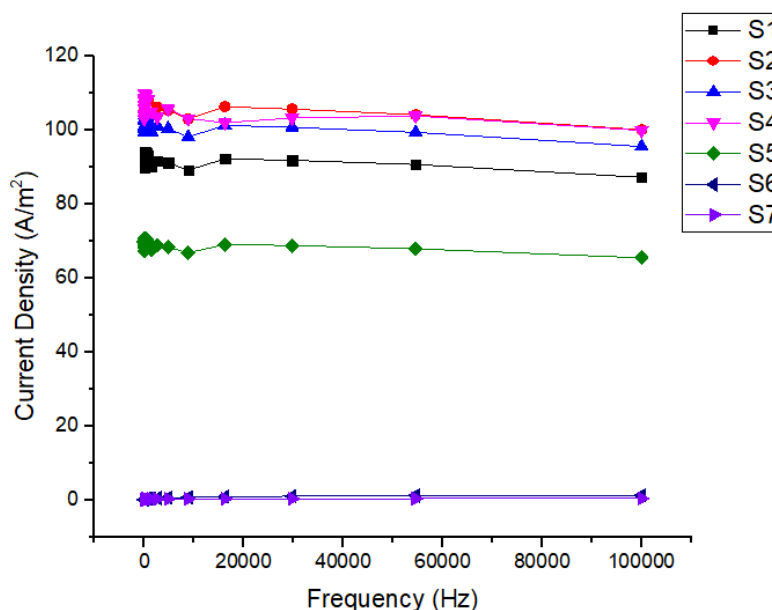
Where Z = the impedance of the NiCo<sub>2</sub>O<sub>4</sub>/rGO nanocomposite (Ω), R = the resistance of the RLC ω circuit, = the angular frequency of the wave propagated in the sample (rad) where ω = 2πf and C = the value of the sample capacitance (Farad). The following are the results of specific capacitance testing using a CV-meter based on an RC circuit.

Figure 7 shows the relationship of specific capacitance with frequency in NiCo<sub>2</sub>O<sub>4</sub>/rGO nanocomposite which has the highest specific capacity regression line in sample S2 of 289.93 F/g. This

indicates that the increase in the mass content of cobalt oxide (Co<sub>3</sub>O<sub>4</sub>) which carries the charge of the Co<sup>2+</sup> ion can expand the specific surface area so that the number of holes for storing free electrons is greater because the active group of Co-OH is bent to form an electron bridge to make free electrons easy to move and oscillate[29]. Based on the results of the literature, the specific capacitance value of the supercapacitor electrode for the pseudocapacitor of the NiCo<sub>2</sub>O<sub>4</sub> material type is 120 F/g [30]. In addition, when the supercapacitor electrode is under an electric field with an energy gap above the band gap of the NiCo<sub>2</sub>O<sub>4</sub>/rGO nanocomposite, the free electron adsorption process occurs so that it can produce electron-hole pairs which can increase the electric current. The following are the results of testing the current density of NiCo<sub>2</sub>O<sub>4</sub>/rGO nanocomposites with respect to the frequency of electric waves exposed from 1 Hz to 10 kHz.



**Figure 7** CV meter results of each sample of Specific Capacitance versus Frequency



**Figure 8** Relationship of Current Density to Frequency in NiCo<sub>2</sub>O<sub>4</sub>/rGO nanocomposites

The relationship between current density and frequency in Figure 8 provides information about the electrolyte and the resistance of charge transfer in the electrolyte. For S2 at a frequency of 100 kHz there is an increase in current density of 105.90 A/m<sup>2</sup>, but at a frequency of 1 Hz there is a decrease in current density. This is due to the difficulty of penetrating the electrical signal into the deeper pores and smaller particles which results in longer electron transfer in the hole, resulting in higher resistance [31]. This is also evidenced by the relationship between current density and specific capacitance which is directly proportional to each other if drawn based on the regression line, the data obtained are shown in Table 9

**Table 9.** Results of Characterization of Specific Capacitance Values and Current Density of NiCo<sub>2</sub>O<sub>4</sub>/rGO Nanocomposites

Sample code	Specific Capacitance (Farad/g)	Current Density (A/m <sup>2</sup> )
S1	106.69	91.84
S2	289.93	106.32
S3	182.59	96.51
S4	277.02	105.87
S5	39.77	68.89
S6	0.11	0.44
S7	0.06	0.21

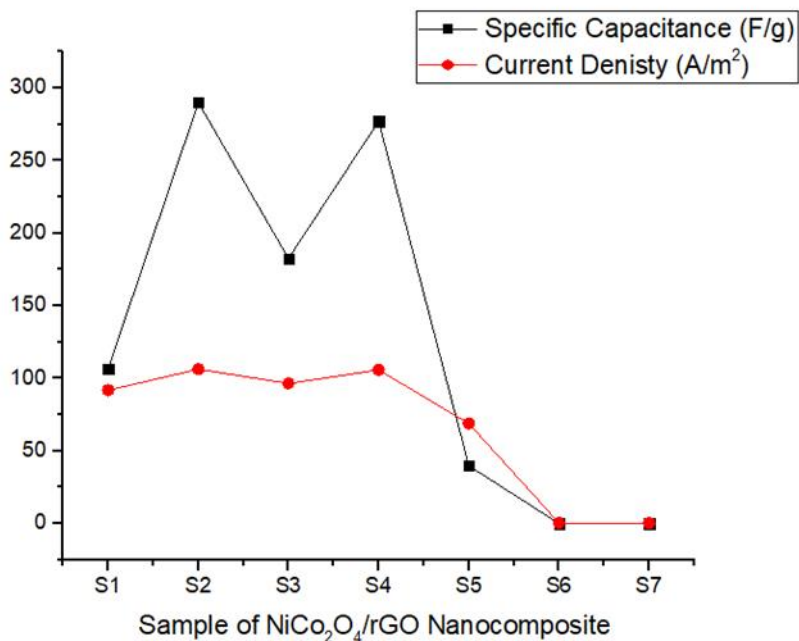
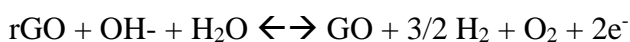
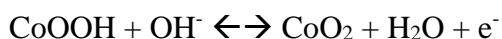
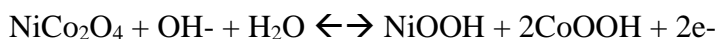


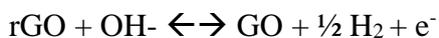
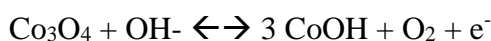
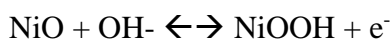
**Figure 9** The Relationship between Current Density and Specific Capacitance in NiCo<sub>2</sub>O<sub>4</sub>/rGO Nanocomposites

The specific capacitance of the NiCo<sub>2</sub>O<sub>4</sub>/rGO nanocomposite supercapacitor increases with increasing current density due to the ability of the supercapacitor electrode particles to diffuse electrolyte ions in the electrode microspores as shown in

Figure 9. In addition, it is also due to the behavior of the supercapacitor electrode performance of the NiCo<sub>2</sub>O<sub>4</sub>/rGO nanocomposite in alkaline electrolytes during the electrochemical process is influenced by an electrochemical process in which the process involves redox reactions which will result in changes in the valence electrons of Co<sup>3+</sup>/Co<sup>4+</sup> and M<sup>2+</sup>/M<sup>3+</sup> (M = Co or Ni) on the surface of the nanocomposite electrode so that the Faradaic reaction is faster and reversible according to the chemical reaction equation below: [32].



Meanwhile, for NiO nanoparticles on the inner surface of the nanocomposite, a Faradaic reaction occurs in an alkaline electrolyte solution which will proceed according to the following equation:



#### 4. CONCLUSIONS

The NiCo<sub>2</sub>O<sub>4</sub>/rGO nanocomposite as the best pseudocapacitive supercapacitor electrode at S2 with a specific surface area of 12.75 m<sup>2</sup>/g, a mean pore radius of 9.534 nm and a pore volume of 0.06404 cm<sup>3</sup>/g and a pretty good performance from the analysis of electrical properties which has an electrical conductivity value of 6.08 S/m and a capacitance of 289.93 F/g. This is evidenced from the analysis of FTIR spectra, the presence of C=C group bonds with sharp peaks and Co-OH, Co-O bonding groups at wave numbers 1627 cm<sup>-1</sup> and 835 cm<sup>-1</sup> which the active groups have cationic properties so that the process of carrying an electric charge is more optimal. In this study, NiCo<sub>2</sub>O<sub>4</sub>/rGO nanocomposites were synthesized through coprecipitation and hydrothermal yielding the optimum composition at S2 with mass variations of NiO, Co<sub>3</sub>O<sub>4</sub> and rGO respectively 2:3:2 with the characteristics of producing a hexahedron surface morphology with an average particle size about 0.005 m<sup>2</sup> and has a spinel crystal structure and a cubic phase where the orientation of the crystal planes are [2 2 0] and [1 1 1] with a crystalline diameter of 0.454 nm composed of the main groups -OH, C=C, CH, Co-OH, Ni-O and Co-O with wave numbers 3448.51 cm<sup>-1</sup>, 1627.77 cm<sup>-1</sup>, 1384.61 cm<sup>-1</sup>, 835.35 cm<sup>-1</sup>, 740.41 cm<sup>-1</sup> and 446.73 cm<sup>-1</sup>, melting point 468<sup>0</sup>C and mass decomposition 63.84%.

#### ACKNOWLEDGMENTS

This research was supported by the 2021 Doctoral Dissertation Research Grant from the Ministry of Research and Technology/National Research and Innovation Agency of the Republic of Indonesia (Kemenristek/BRIN) which has provided funding under SK No: 8/E1/KPT/2021 and Contract Agreement No. 12/E1/KP.PTNBH/2021. Thanks to the Indonesian Research Institute (LIPI) for the experiments process and Physics Laboratory of University of North Sumatra for the synthesis process.

#### References

1. F. Ortenzi, M. Pasquali, P. P. Prosini, A. Lidozzi, M. Di Benedetto, *Energies.*, 12 (2019) 12.
2. E. Umeshbabu, G. Rajeshkhanna, P. Justin, and G. R. Rao, *J. Solid State Electrochem.*, 20 (2016) 2725–2736.
3. Y. Wang, J. Guo, T. Wang, J. Shao, D. Wang, Y.-W. Yang, *Nanomater.*, 5 (2015) 1667–1689.
4. P. H. Yanti, A. Mukhtar, Astarina, *J. Kim.*, 1 (2015) 124–129.
5. X. Chen, R. Paul, and L. Dai, *Natl. Sci. Rev.*, 4 (2017) 453–489.
6. C. Cui, J. Xu, L. Wang, D. Guo, M. Mao, J. Ma, T Wang, *ACS Appl. Mater. Interfaces.*, 8 (2014) 8568–8575.
7. K. Xu, X. Huang, Q. Liu, R. Jou, W. Li, X. Liu, S. Li, J. Yang, J. Hu, *J. Mater. Chem. A.*, 2 (2014) 16731–16739.
8. C. Yuan, J. Li, L. Hou, J. Lin, G. Pang, L. Zhang, L. Lian, X. Zhang, *RSC Adv.*, 3 (2013) 18573–18578.
9. J. Shen, X. Li, N. Li, M. Ye, *Electrochim. Acta.*, 141 (2014) 126–133.
10. M. Srivastava, M. Elias Uddin, J. Singh, N. H. Kim, J. H. Lee, *J. Alloys Compd.*, 590 (2014) 266–276
11. C. Yao, Y. Su, Y. Li, J. Li, *Int. J. Electrochem. Sci.*, 16 (2021) 150917.
12. H. Rao, Z. Zhang, H. Ge, X. Liu, P. Zou, X. Wang, Y. Wang, *New J. Chem.*, 41 (2017)3667–3676.
13. A. K. Das, R. K. Layek, N. H. Kim, D. Jung, J. H. Lee, *Nanoscale.*, 6 (2014) 10657–10665.

14. A. García-Miranda Ferrari, D. A. C. Brownson, C. E. Banks, *ChemElectroChem.*, 6 (2019) 5446–5453.
15. C. Zhang, X. Geng, S. Tang, M. Deng, and Y. Du, *J. Mater. Chem. A*, (5 (2017) 5912–5919.
16. S. Al-Rubaye, R. Rajagopalan, S. X. Dou, Z. Cheng, “*J. Mater. Chem. A.*, 5 (2017) 18989–18997.
17. H. Tong, S. Yue, L. Lu, F. Jin, Q. Han, X. Zhang, *Nanoscale.*, 9 (2017) 16826–16835.
18. L. M. Al-Qirby, S. Radiman, C. W. Siong, A. M. Ali, *Ultrason. Sonochem.*, 38 (2017) 640–651.
19. N. K. Yetim, N. Aslan, A. Sarioğlu, N. Sarı, M. M. Koç, *J. Mater. Sci. Mater. Electron.*, 31 (2020) 12238–12248.
20. X. Ni, Y. Zhang, D. Tian, H. Zheng, X. Wang, *J. Cryst. Growth.*, 306 (2007) 418–421.
21. F. Zhang, C. Yuan, X. Lu, L. Zhang, Q. Che, X. Zhang, *J. Power Sources.*, 203 (2012) 250–256.
22. D. Son, S. Cho, J. Nam, H. Lee, M. Kim, *Polym.*, 12 (2020) 1053.
23. S. Chaudhari, D. Bhattacharjya, J. S. Yu, *Bull. Korean Chem. Soc.*, 36 (2015) 2330–2336.
24. R. Bardestani, G. S. Patience, S. Kaliaguine, *Can. J. Chem. Eng.*, 97 (2019) 2781–2791.
25. Y. Wang, J. Guo, T. Wang, J. Shao, D. Wang, Y. W. Yang, *Nanomaterials.*, 5 (2015) 1667–1689.
26. J. Kim, S.J. Park, S. Kim, *Appl. Chem. Eng.*, 30 (2019) 324–330.
27. P. S. Shewale, K. S. Yun, *Nanomaterials.*, 11 (2021) 852.
28. M. HariPriya, R. Sivasubramanian, A. M. Ashok, S. Hussain, G. Amarendra, *J. Mater. Sci. Mater. Electron.*, 30 (2019) 7497-7506.
29. S. Khalid, C. Cao, L. Wang, Y. Zhu, *Scientific Report.*, 6 (2016) 1-13.
30. N.R. Chodanciar, H. D. Pham, A. K. Nanjundan, J. F. S. Fernando, K. Jayaramulu, D. Golberg, Y. K. Han, D. P. Dubal, *Review of Advance Science News.*, 16 (2020) 1-35.
31. M. Suleman, M. Deraman, M. A. R. Othman, M. Omar, M. A. Hashim, N. H. Basri, N. S. M. Nor, B. N. M. Dolah, M. F. Y. M. Hanappi, E. Hamdan, *Journal of Physics*, 739 (2016) 1-10.
32. S. Mahadik, N. R. Chodankar, Y.-K. Han, D. Dubal, S. Patil, *ChemSusChem*, 14 (2021) 5384